RESEARCH

Assessment of storm-time ionospheric electron density measurements from Spire Global CubeSat GNSS radio occultation constellation

Lei Liu[1] · Y. Jade Morton[1]

Abstract

Spire Global's CubeSats has been collecting global navigation satellite system ionospheric radio occultation (RO) measurements since November 2019. This study presents a comprehensive evaluation of storm-time ionospheric electron density measurements derived from Spire precise orbit determination (POD) antenna by comparing them with measurements obtained from digisonde, incoherent scatter radar (ISR), and the constellation observing system for meteorology, ionosphere, and climate 2 (COSMIC2) mission during February 2020–December 2021. Results showed electron density profiles (EDPs) retrieved from Spire POD antenna are in general agreement with those from digisonde, ISR, and COSMIC2 RO observations, although Spire-retrieved EDPs sometimes are noisier than others. Spire-derived F2 layer peak density (NmF2) and peak height (hmF2) agree well with collocated measurements from digisonde and COSMIC2. The good performance of Spire-derived ionospheric parameters provides a baseline reference for subsequent merged observations from POD and RO antennas and suggests that low-cost CubeSats can provide reliable ionospheric measurements to significantly contribute to global ionospheric monitoring.

Keywords Spire CubeSat · GNSS radio occultation · Ionospheric electron density · NmF2 and hmF2

Introduction

Global navigation satellite system (GNSS) radio occultation (RO) sounding uses GNSS measurements obtained by a low earth orbiting (LEO) satellite to retrieve atmospheric and ionospheric profiles (Hajj and Romans 1998; Schreiner et al. 1999; Yue et al. 2014). It has been proven to be a powerful technique for retrieval of ionosphere electron density profiles (EDPs) with high vertical resolution and global coverage. The Abel inversion algorithm is widely applied to obtain the EDPs, which assumes the spherical symmetry of the electron density field (Schreiner et al. 1999; Mannucci et al. 2020; Angling et al. 2021). Generally, the Abel inversion algorithm can be implemented in two approaches when retrieval of ionospheric EDPs (Schreiner et al. 1999). The first one is based on the bending angle caused by the ionospheric refractive index. The second one is thorough the estimation of total electron content (TEC), assuming the straight-line propagation of GNSS RO signals where elevation angles are below 0°.

Over the past two decades, ionospheric RO products based on the original or improved Abel inversion algorithms have been generated by various GNSS RO missions, such as global position system/meteorology (GPS/MET) (Schreiner et al. 1999), challenging minisatellite payload (CHAMP) (Wickert et al. 2001; Jakowski 2005), scientific application satellite-C (SAC-C) (Hajj et al. 2004; Colomb et al. 2004), gravity recovery and climate experiment (GRACE) (Beyerle et al. 2005), constellation observing system for meteorology, ionosphere, and climate 1 (COSMIC1) and its follow-on mission COSMIC2 (Schreiner et al. 2007; Ho et al. 2020; Chou et al. 2017; Lin et al. 2020), PlanetiQ (Kursinski et al. 2021), GeoOptics (Chang et al. 2022), and Spire Global (Angling et al. 2021).

In particular, Spire Global is a commercial space-to-cloud analytics company that operates more than 120 LEO 3U CubeSats. Currently, more than 40 Spire CubeSats are equipped with low-cost, low-power, and low-mass GNSS receivers which can provide ionospheric RO measurements at low latency to support space weather monitoring (Angling

✉ Lei Liu
   Lei.Liu@colorado.edu

1   Ann and H. J. Smead Aerospace Engineering Sciences
    Department, University of Colorado Boulder, Boulder, CO,
    USA

et al. 2021). However, it is important to evaluate the reliability and feasibility of Spire ionospheric RO-related measurements before they are applied for scientific and assimilative purposes. Forsythe et al. (2020) assessed Spire RO ionospheric electron density measurements by comparing them with collocated digital ionosonde (digisonde) and incoherent scatter radar (ISR) measurements using a limited data set of 14 consecutive geomagnetically quiet days. Results showed that there are good agreements between these independent measurements. This paper extends the work of Forsythe et al. (2020) to implement a comprehensive assessment of ionospheric electron density measurements obtained from the Spire CubeSats POD antennas for all available storm-time Spire RO events during February 17, 2020–December 3, 2021.

The objective of this study is to obtain a baseline performance assessment of the Spire RO ionospheric electron density measurements made under disturbed ionospheric conditions by comparing them with measurements from globally distributed digisonde, ISR, and COSMIC2 observations. Comparisons are also made for collocated ionospheric parameters between Spire RO and the international reference ionosphere (IRI) 2016 model.

Data and methodology

This section describes the retrieval of Spire ionospheric RO data, and the criteria of collocated ionospheric observations between Spire RO and other data sources. Various evaluation metrics are also presented in this section.

Spire ionospheric RO measurements

Currently, Spire Global operates a constellation of more than 120 CubeSats known as LEMURs (low-earth multi-use receivers), and over 40 of them perform radio occultation (RO) measurements from global navigation satellite systems (GNSS) constellations, such as GPS, Galileo, GLONASS, and QZSS. These CubeSats are in low earth orbiting (LEO) planes with various inclinations at altitudes between 400 and 600 km, enabling them to provide global coverage (Angling et al. 2021). The Spire CubeSat is capable of receiving and processing dual-frequency GNSS signals entering three antennas: precise orbit determination (POD), front RO (FRO), and backward RO (BRO) antennas.

The POD antenna receives dual-frequency GNSS signals from both high elevation measurements of the topside ionosphere and low/negative elevation RO measurements of the bottom-side ionosphere. The FRO and BRO antennas mounted on the front and back sides are designed for observing GNSS ionospheric RO measurements with low/negative elevation angles. The Spire RO electron density profile

(EDP) is calculated from dual-frequency GNSS total electron content (TEC) measurements along the LEO-GNSS link based on the Abel inversion algorithm. It should be noted that the Spire TEC profiles observed by the POD antenna are calibrated, whereas those TEC measurements observed by FRO and BRO antennas are uncalibrated due to the CubeSat RO receiver DCB issue (Angling et al. 2021). Therefore, the Spire RO EDP products (ionPrf files) evaluated in this study are inverted only from absolute TEC observations using low-elevation LEO-GPS links collected via the POD antenna. The ionPrf files are located at level 2 (L2) data products that are available from NASA's Commercial Smallsat Data Acquisition (CSDA) program (https://www.earthdata.nasa.gov/esds/csda/commercial-datasets). Each ionPrf file contains an EDP at the location of the RO tangent point trace (longitude, latitude, and altitude). In retrieval of RO EDP, the Abel inversion algorithm assumes the local spherical symmetry in ionospheric densities along the lines of sight between GNSS and LEO satellites. Inversion errors could be introduced when the RO rays go through regions with large horizontal gradients, especially for low latitudes (Schreiner et al. 1999; Chou et al. 2017). It is important to note that an RO-retrieved EDP is not a vertical profile because RO tangent points at different ionospheric heights could be separated by several thousand kilometers depending on the RO geometry (Forsythe et al. 2020; Cherniak et al. 2021).

In this study, we aim at evaluating the storm-time ionospheric EDPs from the POD antenna of Spire RO constellations. A geomagnetic storm is declared if the disturbance storm-time (Dst) index at a given time is smaller than the Dst threshold, which is set as -40 nT in this study. To take into consideration the time delay between a storm commencement and the ionospheric response, we also include 1 day before and 2 days after the Dst index reaches the threshold value. The top panel of Fig. 1 shows the daily number of ionosphere RO events observed by the Spire POD antenna over the storm time from February 17, 2020, to December 3, 2021. The hourly Dst index is plotted on the right axis of this figure. In total, 114 days are regarded as storm days. The red crosses in the zoom-in plot of the top panel show the daily Spire RO EDP counts during November 1–30, 2021, where both storm and quiet days are included. The daily ionPrf counts are around 50–70, and there are no significant count differences between quiet and storm days. The daily counts of storm-time ionosphere RO events from February 17, 2020, to December 3, 2021, decrease over time, with an exception in April and July 2020 (see top panel). The Spire CubeSats number that contributes all available POD RO EDP counts also shares a similar variation trend (see the middle panel), except for April and July 2020. The drop of daily RO EDP counts could likely be due to that fewer Spire CubeSats are generating measurements from the POD antenna those days. The bottom panel of Fig. 1 shows an
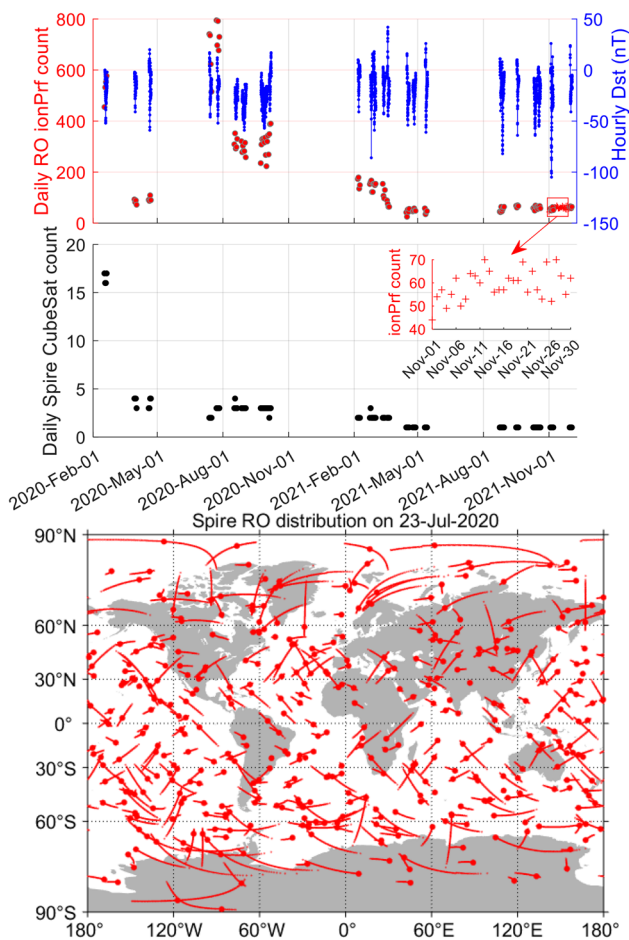
Fig. 1 Spire ionospheric RO distributions. Top panel: time series of daily Spire ionospheric RO events (left axis) and hourly disturbance storm-time (Dst) variations (right axis). Daily ionospheric RO counts from November 1 to 30, 2021, are indicated by the red crosses where both quiet and storm days are included. For better visualization, the related zoom-in figure is plotted below the top panel directed by the red arrow. Middle panel: daily Spire CubeSats number that is used for RO ionPrf generation. Bottom panel: global coverage example of Spire RO on July 23, 2020

example of the geographic distribution of daily Spire RO events on July 23, 2020. This indicates that Spire RO has a global coverage that provides a great opportunity for global ionospheric monitoring.

Note that the number of the POD RO events during the storms is low due to the limited antenna field of view (FOV) which prevents the receiver observations of the lower ionosphere. Only a few Spire CubeSats are configured to track POD antennas to 20 degrees below the local horizontal until February 2022. However, there are about 25 Spire CubeSats that have been producing TEC and EDP by combining overlapping observation arcs of the POD and RO antennas to merge observations from a maximum elevation angle to the lower ionosphere. The merged observations through multiple antennas are currently under evaluation, and the number of

Table 1 Criteria of collocated observations with Spire ionospheric RO traces

Collocated data with Spire RO	Maximum distance separation (km)	Maximum time lapse (minutes)
Digisonde	500	15
COSMIC2 RO		
ISR	1300	10
IRI 2016	N/A	

the daily merged Spire RO events is well over 3000, providing much needed coverage, especially over high latitudes. The quality assessment of the merged measurements is the topic of an ongoing investigation. The results presented in the current submission will serve as a baseline comparison for this future work.

Collocated observations criteria

The evaluation of Spire RO EDP measurements needs nearly simultaneous and collocated observations from other data sources. In this study, collocated observations from all available digisonde stations, ISR, and COSMIC2 are used for comparison with Spire RO-related measurements. Digisonde data are from global ionospheric radio observatory (GIRO) network (https://giro.uml.edu/didbase/scaled.php). COSMIC2 RO data are from COSMIC data analysis and archive center (CDAAC) at the University Corporation for Atmospheric Research (UCAR) (https://data.cosmic.ucar.edu/gnss-ro/cosmic2/). ISR data are from the CEDAR Madrigal database (http://cedar.openmadrigal.org/). Simultaneous and collocated observations are selected empirically based on the distance and time lapse between Spire and other data sources (see Table 1), in a way similar to the threshold defined in previous studies (Lei et al. 2007; Forsythe et al. 2020; Cherniak et al. 2021; Wautelet et al. 2021). The distance bound between digisonde and Spire RO and between COSMIC2 RO and Spire RO is approximately 1104 and 1563 km (see Figs. 4 and 10), respectively. There are only a couple of collocated samples between ISR and Spire RO.

The IRI 2016 model is an empirical ionosphere model depicting ionospheric EDPs between 60 and 2000 km altitude (Bilitza et al. 2017). In this study, electron densities from the IRI 2016 model at the location and time of the Spire RO tangent points are used for baseline comparisons with Spire RO observations since the IRI model cannot capture ionospheric responses to geomagnetic storms.

Evaluation metrics

We use root-mean-square error (RMSE), mean error (ME), and the Pearson correlation coefficient (R) to quantify the

relative performance of the Spire RO-related ionospheric measurements to other reference data sources:

$$
\begin{cases}
\text{RMSE} = \sqrt{\dfrac{1}{N}\sum\limits_{i=1}^{N}(x_{\text{obs},i} - x_{\text{ref},i})^2} \\[3mm]
\text{ME} = \dfrac{1}{N}\sum\limits_{i=1}^{N}\left(x_{\text{obs},i} - x_{\text{ref},i}\right) \\[3mm]
R = \dfrac{\text{cov}\left(x_{\text{obs},i}, x_{\text{ref},i}\right)}{\sigma_{x_{\text{obs},i}} \cdot \sigma_{x_{\text{ref},i}}}
\end{cases}
\tag{1}
$$

where $x_{\text{obs},i}$ is the Spire RO-derived ionospheric observation (e.g., NmF2 and hmF2). $x_{\text{ref},i}$ is the reference value from other data sources at collocated locations, such as digisonde, COSMIC2, and IRI 2016. $i = 1, 2, 3, \dots, N$, and N is the total number of collocated data samples. $\text{cov}\left(x_{\text{obs},i}, x_{\text{ref},i}\right)$ is the covariance between $x_{\text{obs},i}$ and $x_{\text{ref},i}$. $\sigma_{\hat{x}_i}$ and σ_{x_i} are the standard deviations of $x_{\text{obs},i}$ and $x_{\text{ref},i}$, respectively.

Results

This section presents a comprehensive evaluation of Spire-derived ionospheric electron density measurements data by comparing them with collocated measurements obtained from digisonde, ISR and COSMIC2, respectively.

Comparison with digisonde data

Figure 2 compares EDP obtained from Spire RO and nearby digisonde stations on February 18, 2020, around 14:13–14:25 UT. A geomagnetic storm occurred on this day and the Dst reached − 37. The retrieved EDP from digisonde stations agrees well with that from the Spire RO observations, especially for the ionospheric height below 250 km. There is a slight difference between the two instruments on the topside ionosphere, which could be due to extrapolation errors in the digisonde-derived EDP above the F2 layer. It should be noted that the Spire RO EDP is noisier compared to the digisonde measurements. Therefore, data calibration, such as the local regression and Chapman function fitting (Lei et al. 2007; Wautelet et al. 2021; Liu et al. 2019b), is suggested to be performed on Spire RO EDP products, especially for distorted profiles. The black curve shown in the right panel is the local regression fitting result from the original Spire RO EDP (red curve). The noise presented in the original Spire EDP is levelled out well after calibration. Moreover, there are clear fluctuations above the F-region (300–400 km) in the fitted Spire EDP. We believe these fluctuations are due to the presence of irregularities there.

In this section, we assess the quality of two important ionospheric parameters (NmF2 and hmF2) retrieved from Spire RO measurements by comparing them with globally distributed GIRO-derived digisonde F2 peak parameters. Figure 3 shows all available collocated observations from Spire RO and digisondes during storm days from February 17, 2020, to December 3, 2021. The available digisonde
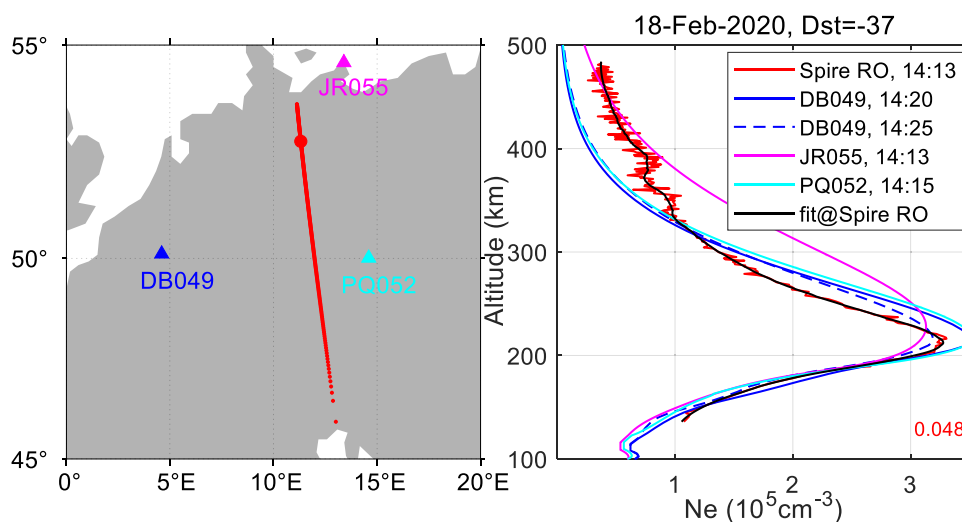

Fig. 2 An example of spire RO electron density (Ne) profiles as compared with collocated digisonde observations. Left panel: red curves represent Spire RO tangent point track. (Red dot shows the NmF2 location.) Triangles indicate the location of three digisondes that are in the vicinity of the Spire RO trace. Right panel: storm-time EDP from digisondes and Spire RO near 14:13–14:25 UT are represented by different colors. The black curve in the right panel is the smoothed result from the original Spire RO EDP (red curves) using the local regression fitting. The root-mean-square error (RMSE) of the Spire EDP is marked at the right-bottom corner of the right panel with the unit of $\llbracket 10 \rrbracket ^5 \llbracket cm \rrbracket ^{(-3)}$, which is calculated from the difference between the original and fitted Spire EDP
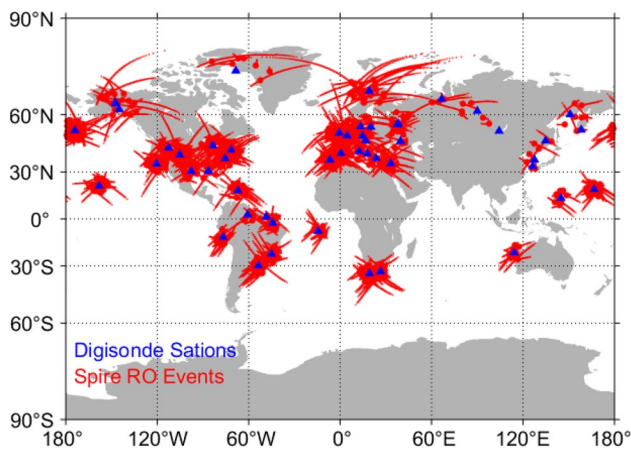
Fig. 3 Geographic distribution of collocated observations from Spire RO events and digisonde stations covered by the storm days during February 17, 2020–December 3, 2021. Red curves and blue triangles indicate the distribution of Spire RO events and digisonde stations, respectively

station number is 54. There are a total of 1104 collocated data samples between Spire RO and digisonde stations.

Figure 4 shows a statistical comparison of the storm-time Spire RO-derived NmF2 with collocated digisonde observations and IRI 2016 estimations. Evaluation metrics are listed in the plots. There are 1104 collocated storm-time NmF2 points. The Spire RO-derived NmF2 values are in close agreement with those from digisonde/IRI as evident in the very small RMSE ($1.07/1.36 \times 10^5 \mathrm{cm}^{-3}$) and ME ($-0.15/0.10 \times 10^5 \mathrm{cm}^{-3}$), and high correlation coefficient values (0.94/0.90) between them. In this study, the NmF2 correlation coefficient value between Spire RO measurements and digisonde data is comparable with that shown in Forsythe et al. (2020) where a good correlation of 0.96 is obtained over 14 consecutive geomagnetically quiet days. In comparison with the statistical result for COSMIC

satellites, the NmF2 correlation coefficient shown in this study is slightly better than that in Lei et al. (2007) where a correlation coefficient of 0.85 with 276 collocated points was shown. However, the Spire NmF2 correlation coefficient in this study is slightly lower than the one presented by Krankowski et al. (2011) who showed a correlation coefficient of 0.99 using 750 collocated COSMIC RO events distributed over the European region.

Figure 5 shows similar scatter plots for hmF2 comparisons. The Spire RO-derived hmF2 shows a clear linear relationship with those from digisonde observations and IRI 2016 model. However, the RMSE and ME between Spire RO and digisonde are 27.13 km and −7.71 km, which are smaller than that between Spire RO and IRI 2016 observations. Also, the correlation coefficient between Spire RO and digisonde (0.82) is higher than that between Spire RO and IRI 2016 observations (0.76). This could be partly due to IRI 2016 being a climatology model which cannot capture the day-to-day variability of the ionosphere, especially on storm days (Bilitza et al. 2017; Liu et al. 2019a; Chen et al. 2020).

Comparison with ISR electron density profiles

Unlike digisondes, an ISR provides ionospheric profiles that can extend to the top side. Unfortunately, only a couple of collocated quit-time samples over Millstone Hill (Fig. 6) and Poker Flat (Fig. 7) stations are available after searching globally distributed ISR observations from the CEDAR Madrigal database.

In Fig. 6, Spire RO-retrieved electron density profiles (red curves) are compared with the Millstone Hill ISR measurements. The ISR measurements over Millstone Hill are from the Zenith antenna operated via the alternate code (AC, blue dots) and single pulse (SP, magenta dots) modes, respectively. There are two Spire RO tracks (see Spire (1) and Spire (2) in panel (a)) that are close to Millstone Hill station.

Fig. 4 Scatter plots of the storm-time Spire RO NmF2 against available digisonde measurements (left panel) and IRI 2016 (right panel), respectively. The black solid line shows the best-fit line. There are 1104 collocated storm-time NmF2 points that are selected from February 17, 2020, to December 3, 2021
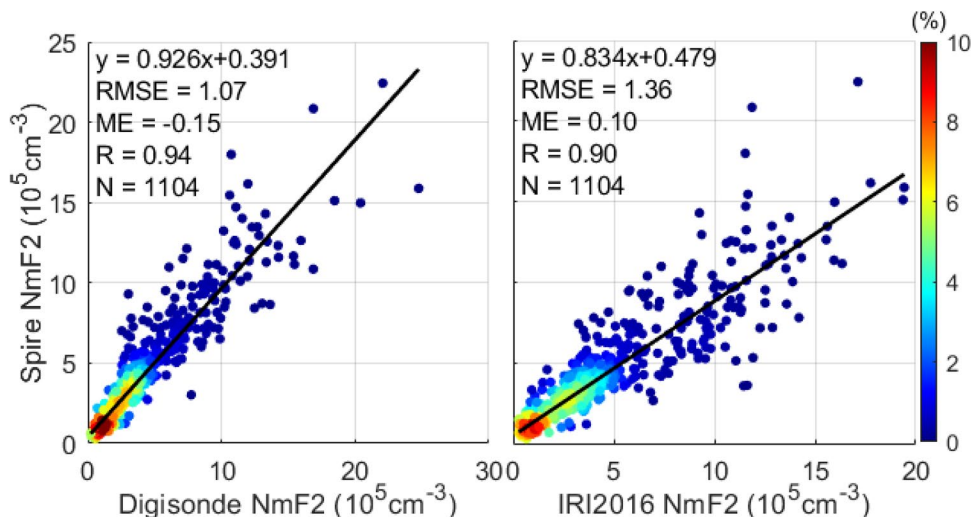
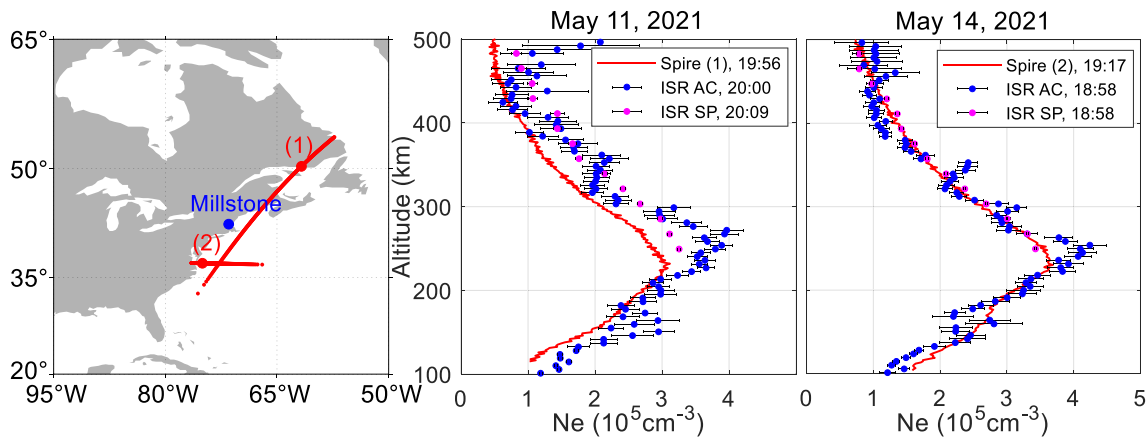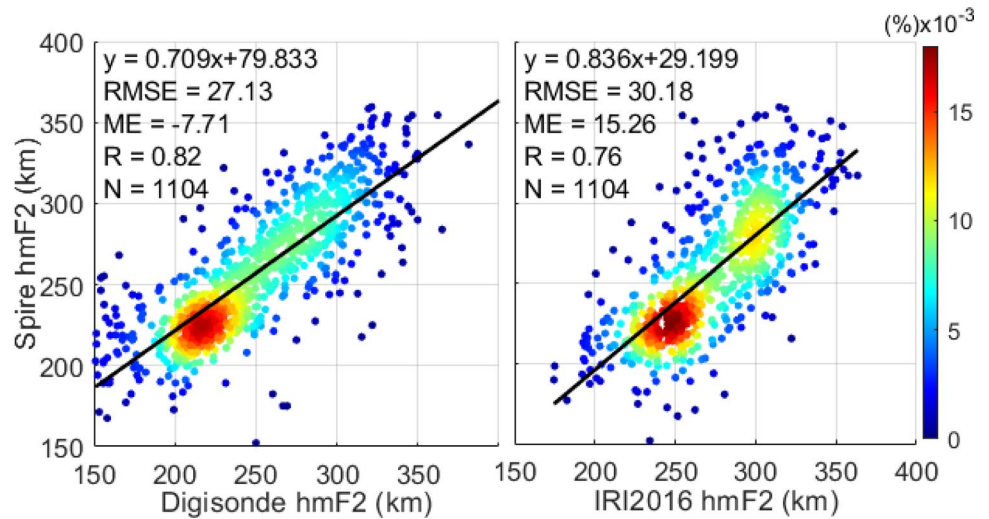**Fig. 5** Similar to Fig. 4, but for hmF2 comparison

Fig. 6 Comparison of spire RO Ne with those measured by Millstone Hill incoherent scatter radar (ISR) station. Left panel: red curves represent Spire RO tracks with NmF2 locations (red dots). Blue dots represent the nearby ISR station. Middle and right panels: Ne profiles May 11 and 14, 2021, respectively. Spire Ne profiles are indicated by red curves. The ISR Ne measurements from alternate code (AC) and single pulse (SP) modes are represented by blue and magenta dots, respectively
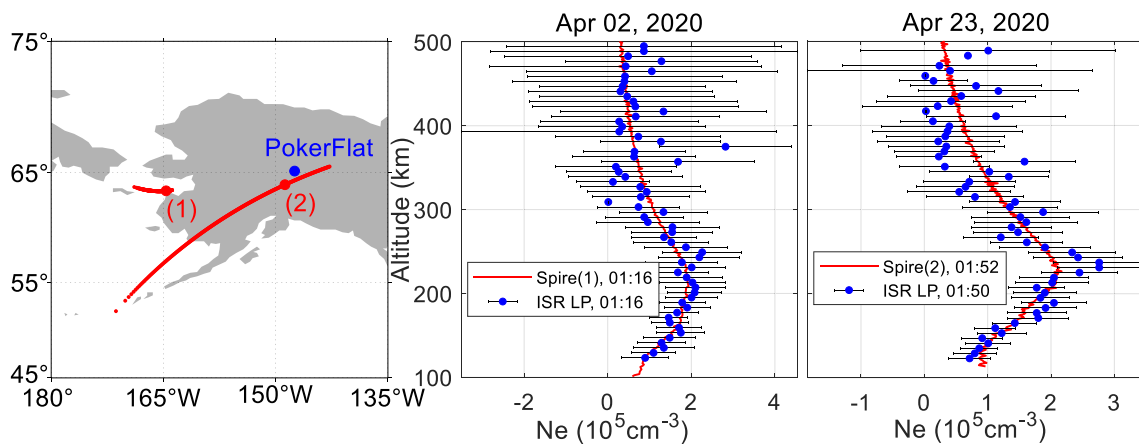
Fig. 7 Similar to Fig. 6, but comparison with the Poker Flat ISR long pulse (LP) mode Ne measurements

EDPs from the Spire RO and Millstone Hill ISR show good agreement over a wide range of altitudes (see panels (b) and (c)). However, there is a notable difference near the (NmF2, hmF2) location, especially in panel (b), which is probably a result of the large horizontal ionosphere gradients because the Spire (1) RO track is separated by several thousands of kilometers.

Figure 7 shows two more Ne samples comparison between Spire RO and Poker Flat ISR. The Poker Flat ISR measurements used here are operated in the long pulse (LP) mode from the zenith antenna. The profiles from Spire RO and ISR follow each other very well, though the error bars of the ISR electron density profiles are somewhat large.

Comparison with COSMIC2 RO observations

Figure 8(a) shows all collocated RO tracks between Spire and COSMIC2 on February 18, 2020, where the minimum Dst index is below − 50. In total, there are 26 collocated RO events on this day. Figure 8b–e shows four examples of collocated EDPs marked by letters "(b), (c), (d), and (e)" in Fig. 8a, respectively. In general, the EDPs from Spire RO and COSMIC2 RO show excellent agreement from the bottom to the topside ionosphere during storm time. The storm-time NmF2 and hmF2 from collocated Spire and COSMIC2 observations also agree well. In Fig. 8a, the E layer altitude (around 140 km) from the Spire RO and COSMIC2 RO

Fig. 8 Collocated RO iono-spheric electron density observations between Spire (red dots) and COSMIC2 (blue dots) missions on a storm day (February 18, 2020). The smoothed results from Spire and COSMIC2 RO EDPs are indicated by the black and magenta curves, respectively, which are referred as truth in calculation of root-mean-square error (RMSE) in this study. The RMSE for Spire (red number) and COMSIC2 (blue number) is illustrated at the right-bottom corner of each panel with the unit of $[\![10]\!]^5$ $[\![cm]\!]^{(-3)}$. IRI-derived electron densities (gray curves) are also calculated at locations of Spire RO tracks. The Dst index is marked at the top of each panel
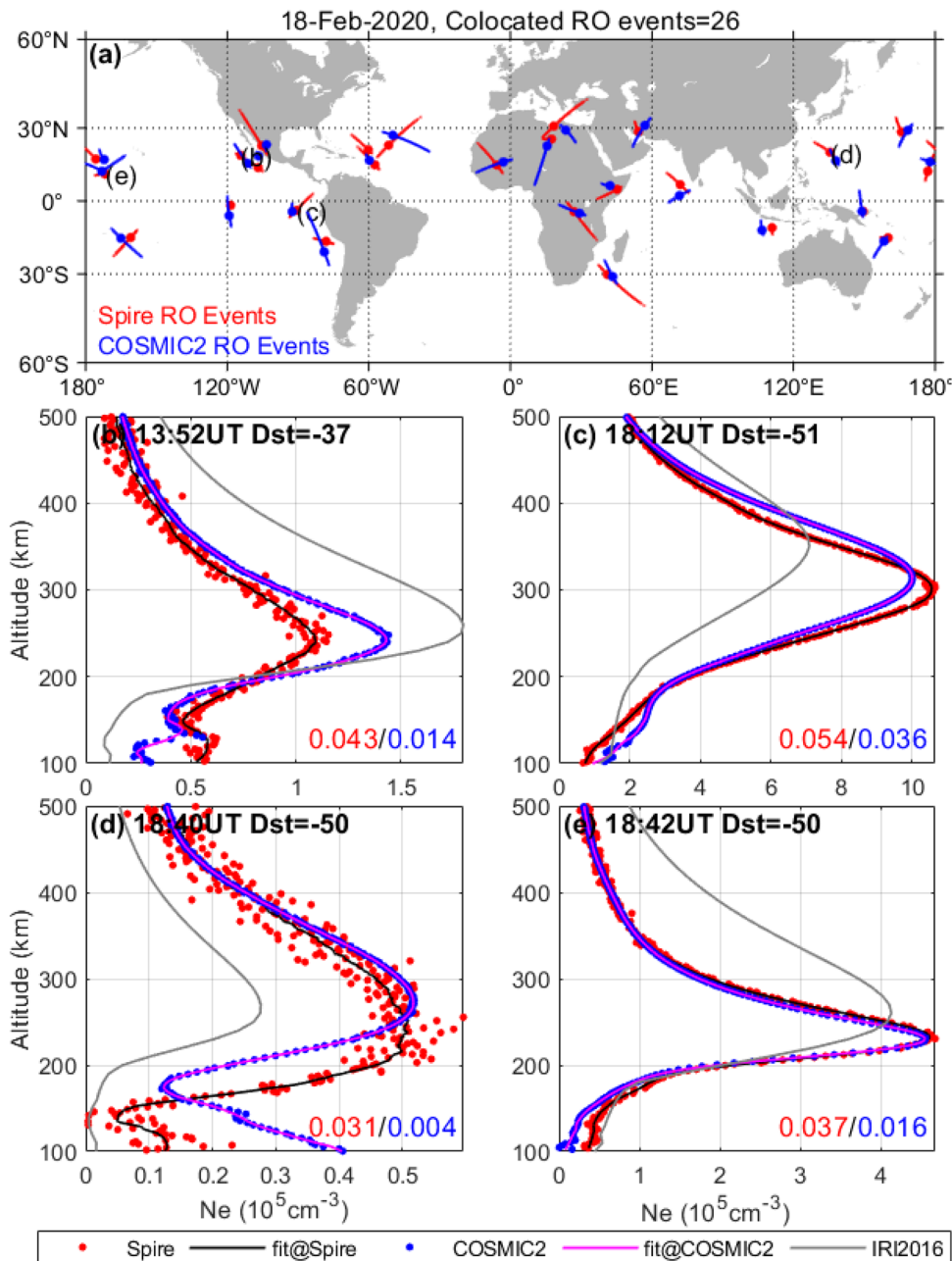
observations also agrees with each other. Black curves in panels (b), (c), (d) and (e) are the fitting results from the Spire RO EDPs (red curves). It is clear that the smoothed Spire RO EDPs are less noisy than the original ones. The Spire RO EDPs are noisier than that from COSMIC2 as the RMSE errors from the Spire are larger than the COSMIC2.
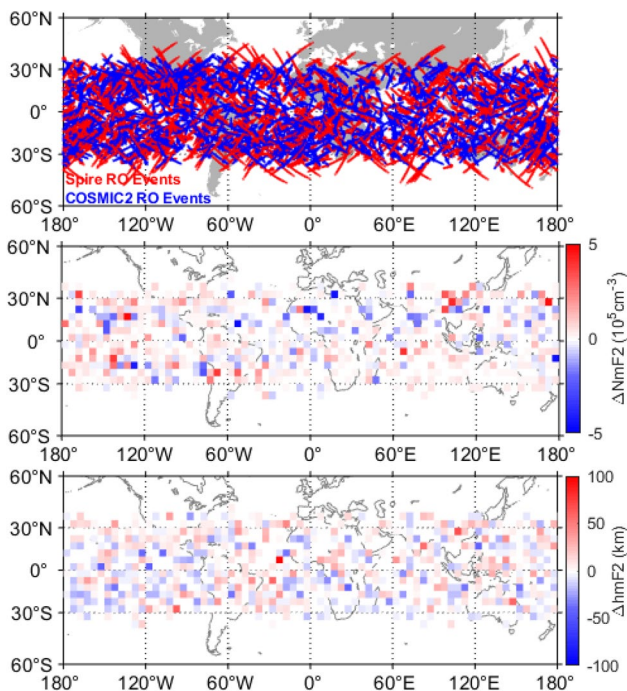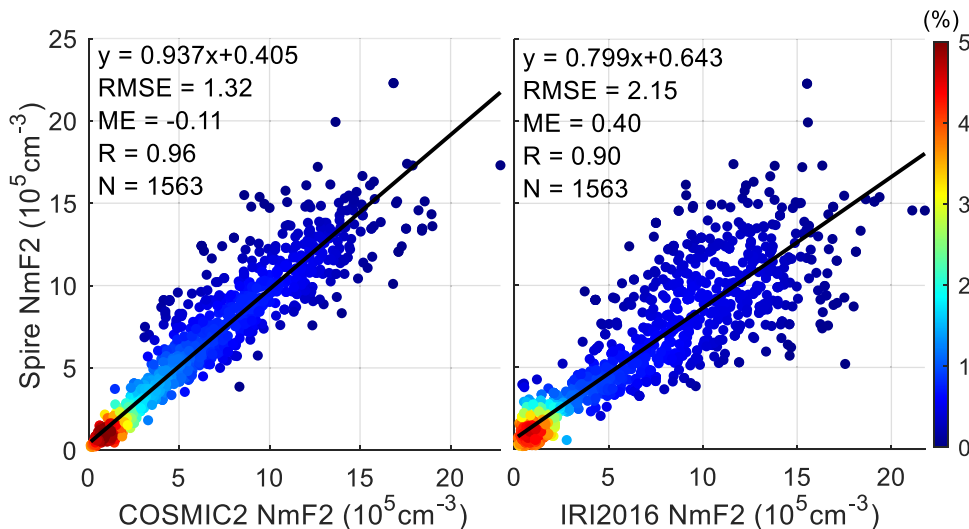
Spire RO EDPs for each panel share the same levels of noises because their RMSE errors are commonly around $0.03 - 0.05 \times 10^5 cm^{-3}$. The illusion of noise differences from Spire RO EDPs between panels (b), (d) and (c), (e) is probably due to that they are plotted in different scales of the horizontal axis. There are some nonnegligible differences between RO-derived EDPs and IRI 2016 model. This is understandable because IRI 2016 is an empirical and climatological model without the capability of reproducing storm-time variability in the ionosphere.

The top panel of Fig. 9 shows the geographical distribution of the collocated Spire (red curves) and COSMIC2 (blue curves) RO tracks during the storm days from February 17, 2020, to December 3, 2021. The corresponding mean $\Delta NmF2$ and $\Delta hmF2$ maps are presented in the middle and bottom panels of Fig. 9 using $5° \times 5°$ bins, respectively. $\Delta NmF2$ and $\Delta hmF2$ are uniformly distributed on the maps with their differences mostly limited to $4 \times 10^5 cm^{-3}$ and 50 km, respectively. This indicates that there is a good visual agreement of both NmF2 and hmF2 parameters between Spire and COSMIC2 RO results.

Figure 10 presents scatter plots of the storm-time Spire RO-derived NmF2 against the collocated COSMIC2 observations (left panel) and IRI 2016 estimations (right panel). Evaluation metrics are included at the upper-left location of each panel. There are 1163 collocated storm-time NmF2 points from February 17, 2020, to December 3, 2021. The NmF2 RMSE/ME values between Spire and COSMIC2 are $1.32/ - 0.11 \times 10^5 cm^{-3}$, and the correlation coefficient is around 0.96. This means that there are excellent agreements with a strong linear correlation between the collocated NmF2 derived from the Spire and COSMIC2 missions. Moreover, the Spire RO-derived NmF2 is much closer to those from COSMIC2 than IRI 2016 as there is a slightly

Fig. 9 Global distribution maps of collocated ionospheric RO between Spire and COSMIC2 missions for the storm days defined in Sect. "Spire ionospheric RO measurements." Top panel: red and blue curves indicate the tangent point tracks from Spire and COSMIC2, respectively. Middle and bottom panels: averaged $\Delta NmF2$ and $\Delta hmF2$ maps with a spatial resolution of $5° \times 5°$ bin between Spire and COSMIC2

Fig. 10 Scatter plots of the storm-time Spire RO NmF2 against available COSMIC2 measurements (left panel) and IRI 2016 (right panel), respectively. The black line shows the best-fit line. There are 1163 collocated storm-time NmF2 points which are selected from February 17, 2020, to December 3, 2021
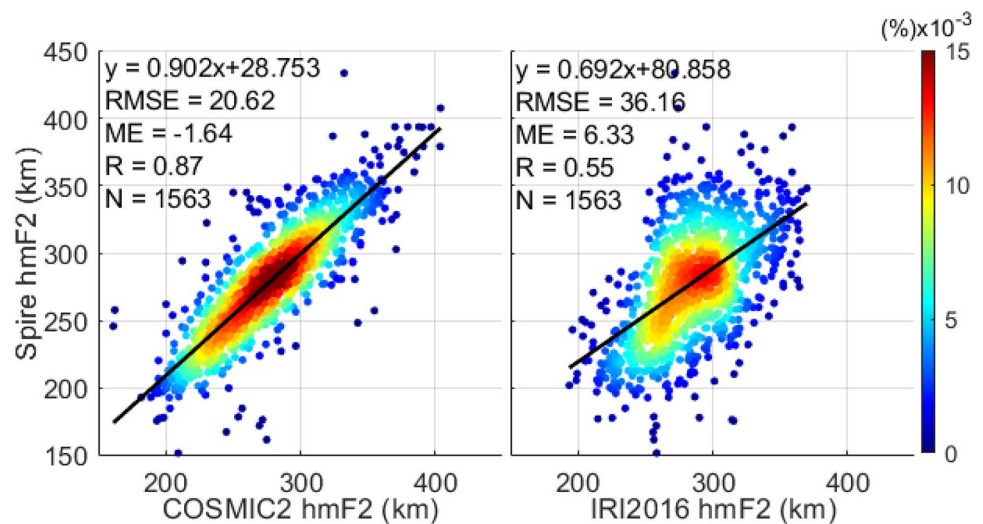
Fig. 11 Similar to Fig. 10, but for hmF2 comparison

higher correlation coefficient value and smaller RMSE/ME errors from COSMIC2 than IRI 2016 model.

A similar comparison for hmF2 is shown in Fig. 11. Good agreements can be also observed from the hmF2 parameters between Spire and COMSIC2 because there are small RMSE/ME (20.62/− 1.64 km) values and a high correlation coefficient (0.87). Spire NmF2 and COSMIC NmF2 follow the same linear trend with small RMSE/ME errors. However, the scattered hmF2 distribution between Spire and IRI 2016 is sparser with increased RMSE/ME values and degraded correlation coefficient value when compared to matched observations from Spire and COSMIC2.

Conclusions

In this study, we present the first performance assessment of storm-time Spire RO electron density measurements by comparing with those from globally distributed 54 digisonde stations, two ISR stations, and the COSMIC2 RO mission. The analysis is performed on geomagnetic storm days from February 2020 to December 2021.

1) The EDPs retrieved from Spire CubeSat GNSS RO agree well with those observed by digisonde, ISR, and COSMIC2 observations, though Spire RO EDPs sometimes are noisier than other data sources.

2) Spire RO-derived NmF2 parameters show strong agreements with those from digisonde/COSMIC2 observations, with low RMSE ($1.07/1.32 \times 10^5 \text{cm}^{-3}$) and ME ($-0.15/ -0.11 \times 10^5 \text{cm}^{-3}$) errors, and high correlation coefficients (0.94/0.96).

3) Good agreements are also shown from the hmF2 comparisons between Spire and digisonde/COSMIC2 as

there are insignificant RMSE (27.13/20.62 km) and ME (− 7.71/− 1.64 km) errors, and high correlation coefficients (0.82/0.87) between them.

4) The comparison of Spire RO-derived ionospheric measurements with IRI 2016 is intended to serve as a baseline check. Our results show that there is a noticeable difference between them as expected because IRI 2016 is an empirical model without the capability of reproducing storm-time variability in the ionosphere.

5) The analysis of Spire ionPrf products suggests that the Spire 3U CubeSats equipped with low-cost, low-power, and low-mass GNSS receivers could provide reliable global-scale ionospheric RO measurements. It should be noted that the Spire RO EDP products assessed in this study are collected from the POD antenna only. An ideal approach to produce Spire EDPs is to combine overlapping observation arcs of both the POD and RO antennas, so that the arcs can span from a maximum elevation angle to the lower ionosphere. Evaluation is underway on these merged Spire EDPs. The current work will serve as a baseline reference for the merged EDP performance analysis.

edu/didbase/scaled.php). The ISR data are from the CEDAR Madrigal database (http://cedar.openmadrigal.org/). The COSMIC2 RO data are from COSMIC Data Analysis and Archive Center (CDAAC) at the University Corporation for Atmospheric Research (UCAR) (https://data.cosmic.ucar.edu/gnss-ro/cosmic2/). The Dst data are obtained from the OMNI Goddard Flight Center (https://omniweb.gsfc.nasa.gov/). The source code of the IRI 2016 model is available online (https://irimodel.org/).

Declarations

Conflict of interest   The authors declare no competing interests.

References

Angling MJ, Nogués-Correig O, Nguyen V, Vetra-Carvalho S, Bocquet FX, Nordstrom K, Melville SE, Savastano G, Mohanty S, Masters D (2021) Sensing the ionosphere with the Spire radio occultation constellation. J Space Weather Space Clim 11:56. https://doi.org/10.1051/swsc/2021040

Beyerle G, Schmidt T, Michalak G, Heise S, Wickert J, Reigber C (2005) GPS radio occultation with GRACE: atmospheric profiling utilizing the zero-difference technique. Geophys Res Lett 32:L13806. https://doi.org/10.1029/2005GL023109

Bilitza D, Altadill D, Truhlik V, Shubin V, Galkin I, Reinisch B, Huang X (2017) International reference ionosphere 2016: from ionospheric climate to real-time weather predictions. Space Weather 15(2):418–429. https://doi.org/10.1002/2016SW001593

Chang H, Lee J, Yoon H, Morton Y, Saltman A (2022) Performance assessment of radio occultation data from GeoOptics by comparing with COSMIC data. Earth Planets Space 74(1):1–17. https://doi.org/10.1186/s40623-022-01667-6

Chen M, Liu L, Xu C, Wang Y (2020) Improved IRI-2016 model based on BeiDou GEO TEC ingestion across China. GPS Solut 24(1):1–11. https://doi.org/10.1007/s10291-019-0938-8

Cherniak I, Zakharenkova I, Braun J, Wu Q, Pedatella N, Schreiner W, Weiss J-P, Hunt D (2021) Accuracy assessment of the quiet-time ionospheric F2 peak parameters as derived from COSMIC-2 multi-GNSS radio occultation measurements. J Space Weather Space Clim 11(2021):18. https://doi.org/10.1051/swsc/2020080

Chou MY, Lin CC, Tsai HF, Lin CY (2017) Ionospheric electron density inversion for global navigation satellite systems radio occultation using aided Abel inversions. J Geophys Res Space Physics 122(1):1386–1399. https://doi.org/10.1002/2016JA023027

Colomb FR, Alonso C, Hofmann C, Nollmann I (2004) SAC-C mission, an example of international cooperation. Adv Space Res 34(10):2194–2199

Forsythe VV, Duly T, Hampton D, Nguyen V (2020) Validation of ionospheric electron density measurements derived from Spire CubeSat constellation. Radio Sci 55(1):e2019RS006953. https://doi.org/10.1029/2019RS006953

Hajj GA, Romans LJ (1998) Ionospheric electron density profiles obtained with the global positioning system: results from the GPS/MET experiment. Radio Sci 33(1):175–190. https://doi.org/10.1029/97RS03183

Hajj GA et al (2004) CHAMP and SAC-C atmospheric occultation results and intercomparisons. J Geophys Res Atmos. https://doi.org/10.1029/2003JD003909

Ho S et al (2020) The COSMIC/FORMOSAT-3 radio occultation mission after 12 years: accomplishments, remaining challenges, and potential impacts of COSMIC-2. Bull Am Meteorol Soc 101(7):E1107–E1136. https://doi.org/10.1175/BAMS-D-18-0290.1

Jakowski N (2005) Ionospheric GPS radio occultation measurements on board CHAMP. GPS Solut 9:88–95. https://doi.org/10.1007/s10291-005-0137-7

Krankowski A, Zakharenkova I, Krypiak-Gregorczyk A et al (2011) Ionospheric electron density observed by FORMOSAT-3/COSMIC over the European region and validated by ionosonde data. J Geod 85:949–964. https://doi.org/10.1007/s00190-011-0481-z

Kursinski E, Brandmeyer J, Botmick A, Leidner M, Leroy S, Gooch R (2021) Initial validation of PlanetiQ ionosphere measurements via comparisons with COSMIC-2 and IRI. In: AGU Fall Meeting Abstracts, vol 2021, pp SA35E-1941

Lei J et al (2007) Comparison of COSMIC ionospheric measurements with ground-based observations and model predictions: preliminary results. J Geophys Res 112:A07308. https://doi.org/10.1029/2006JA012240

Lin CY, Lin CCH, Liu JY, Rajesh PK, Matsuo T, Chou MY, Tsai HF, Yeh WH (2020) The early results and validation of FORMOSAT-7/COSMIC-2 space weather products: global ionospheric specification and Ne-aided Abel electron density profile. J Geophys Res Space Phys 125(10):e2020JA028028. https://doi.org/10.1029/2020JA028028

Liu L, Yao Y, Zou S, Kong J, Shan L, Zhai C, Zhao C, Wang Y (2019a) Ingestion of GIM-derived TEC data for updating IRI-2016 driven by effective IG indices over the European region. J Geod 93:1911–1930. https://doi.org/10.1007/s00190-019-01291-5

Liu JY, Chen CY, Sun YY, Lee IT, Chum J (2019b) Fluctuations on vertical profiles of the ionospheric electron density perturbed by the March 11, 2011 M9.0 Tohoku earthquake and tsunami. GPS Solut 23(76):1–10. https://doi.org/10.1007/s10291-019-0866-7

Mannucci AJ, Ao CO, Williamson W (2020) GNSS radio occultation. position, navigation, and timing technologies in the 21st century: integrated satellite navigation. Sens Syst Civ Appl 1:971–1013. https://doi.org/10.1002/9781119458449.ch33

Schreiner WS, Sokolovskiy SV, Rocken C, Hunt DC (1999) Analysis and validation of GPS/MET radio occultation data in the ionosphere. Radio Sci 34(4):949–966. https://doi.org/10.1029/1999RS900034

Schreiner W, Rocken C, Sokolovskiy S, Syndergaard S, Hunt D (2007) Estimates of the precision of GPS radio occultations from the COSMIC/FORMOSAT-3 mission. Geophys Res Lett 34:L04808. https://doi.org/10.1029/2006GL027557

Wautelet G, Hubert B, Gérard JC, Immel TJ, Frey HU, Mende SB, Kamalabadi F, Kamaci U, England SL (2021) First ICON-FUV Nighttime NmF2 and hmF2 comparison to ground and space-based measurements. J Geophys Res Space Phys 126(11):e2021JA029360. https://doi.org/10.1029/2021JA029360

Wickert J et al (2001) Atmosphere sounding by GPS radio occultation: first results from CHAMP. Geophys Res Lett 28(17):3263–3266. https://doi.org/10.1029/2001GL013117

Yue X, Schreiner WS, Pedatella N, Anthes RA, Mannucci AJ, Straus PR, Liu JY (2014) Space weather observations by GNSS radio occultation: from FORMOSAT-3/COSMIC to FORMOSAT-7/COSMIC-2. Space Weather 12(11):616–621. https://doi.org/10.1002/2014SW001133

Lei Liu is a Research Associate for the Satellite Navigation and Sensing Laboratory at the University of Colorado Boulder. He received his PhD in Geodesy and Geomatics from Wuhan University China in 2020. His current research interests are GNSS ionospheric radio occultation and machine learning in space weather.

Y. Jade Morton is the Helen and Hubert Croft Professor of Engineering in the Smead Aerospace Engineering Sciences Department at the University of Colorado (CU), Boulder. Her research interests lie at the intersection of satellite navigation technologies and remote sensing of the earth's ionosphere, atmosphere, and surface. Dr. Morton received her PhD in electrical engineering from Penn State and was an electrical engineering professor at Colorado State University and Miami University prior to join CU in 2017. Dr. Morton is an Institute of Navigation (ION) Thurlow, Burka and Kepler award winner, an IEEE PLANS Kershner award winner, and an IEEE AESS Distinguished Lecturer. She is a fellow of IEEE, the ION, and the Royal Institute of Navigation (RIN).